Available online at www.sciencedirect.com
SCIENCE DIRECT®
International Journal of Heat and Mass Transfer 48 (2005) 1760–1771
International Journal of HEAT and MASS TRANSFER
www.elsevier.com/locate/ijhmt

Thermal efficiency of near-wall gas-droplet screens II. Experimental study and comparison with numerical results

V.I. Terekhov *, M.A. Pakhomov [1], K.A. Sharov [2], N.E. Shishkin [3]

Kutateladze Institute of Thermophysics SB RAS, 1, Acad. Lavrent'ev Avenue, 630090 Novosibirsk, Russia

Received 16 November 2004
Available online 1 February 2005

Abstract

Results of an experimental study of thermal efficiency of near-wall gas-droplet screens are reported. A description of the experimental setup and procedure used to measure characteristics of interest is given. Deposition of droplet from near-wall gas-droplet jets under isothermal conditions and the effects due to the temperature of the co-current flow, the velocity ratio m, and the thermophysical properties of the vapor–liquid component of the two-phase jet, are examined. A comparison with modeling data is given.

1. Introduction

The reported experimental studies of near-wall gas-droplet screens are few in number [1–6].

A first experimental study of the thermal efficiency of gas-droplet screens behind a tangential slot was reported in [1]. With a two-phase carbon dioxide (CO_2) jet injected into a single-phase nitrogen flow with temperature $T_0 \approx 800$ K and initial turbulence level $Tu_0 = 1.6$–14%, an appreciable (by a factor of 2) gain in the cooling efficiency was obtained over the region where the flow remained two-phase, followed by rapid reduction of this quantity over the length of the channel where the passage to the single-phase regime occurred. The authors of [1] concluded that the use of two-phase coolants in organizing screen systems was more advantageous compared to single-phase flows, and pointed out to an extreme importance of further studies in this research field.

A more systematic study of the cooling efficiency of two-phase screens was reported in [2,3], where the effects due to liquid-phase concentration in the near-wall jet, thermophysical properties of the vapor–liquid component, and inclination angle of the slot through which the jet was injected into the main flow, were examined. The experiments were carried out in a horizontal channel of rectangular cross-section. On the whole, the experimental data were found to be in a good agreement with the results gained within the integral numerical approaches developed in [2,4]. Yet, all experiments in [2,3] were performed at a fixed flow temperature, $T_0 = 50$ °C, and for comparatively low concentrations of liquid droplets (below 2 wt.%).

The efficiency of gas–liquid screens in the maximum possible range of liquid concentrations (0–100%) was examined in [5]. The tests were performed in a

* Corresponding author. Tel.: +7 3832 341736/328969; fax: +7 3832 343480.
E-mail addresses: terekhov@itp.nsc.ru (V.I. Terekhov), pakhomov@ngs.ru (M.A. Pakhomov), sharov@itp.nsc.ru (K.A. Sharov), shishkin@itp.nsc.ru (N.E. Shishkin).
[1] Tel.: +7 3832 391336/244079; fax: +7 3832 343480.
[2] Tel.: +7 3832 391335/417928; fax: +7 3832 343480.
[3] Tel.: +7 3832 391335/322504; fax: +7 3832 343480.

0017-9310/$ - see front matter © 2005 Elsevier Ltd. All rights reserved.
doi:10.1016/j.ijheatmasstransfer.2004.11.011

Nomenclature

A_S area of annular slot (m^2)
$C_{p_a}, C_{p_L}, C_{p_{mx}}$ specific heat capacities of air, liquid, and mixture (J/kg °C)
D channel diameter (m)
g gravity acceleration (m/s^2)
F frequency (Hz)
G_a, G_L mass rate of gas and liquid flows (kg/s)
h, h_{ins} wall thickness and insulated-layer thickness (m)
L length (m)
$m = \rho_S U_S/\rho_0 U_0$ injection ratio
M_L mass concentration of liquid in the gas–liquid mixture
q heat flux (W)
R pipe radius (m)
$Re = U_0 x/\nu$ Reynolds number
$Re_S = U_S s/\nu$ Reynolds number based on the slot height
$Re_L = \Gamma/\nu_L$ liquid-film Reynolds number
S slot height (m)
U_0, U_S main-flow velocity and flow velocity at the slot exit plane (m/s)
T_0, T_S, T_w main-flow temperature, secondary-flow temperature, and adiabatic-wall temperature (°C)
t time (s)
Tu turbulence intensity (%)
x horizontal coordinate (m)
x/S dimensionless coordinate
y wall-normal coordinate (m)

Greek symbols
δ height of liquid film (m)
Φ spectral energy density of waves (m^2/s)
$\Gamma = G_L/\rho_L \cdot \pi D$ volumetric flow rate per unit perimeter (m^2/s)
Γ/Γ_S dimensionless flow rate
μ dynamic viscosity ($(Ns)/m^2$)
ν, ν_L kinematic viscosity of gas and liquid (m^2/s)
$\Theta = (T_0 - T_w)/(T_0 - T_S)$ relative thermal efficiency
$\Theta_L = (T_0 - T_{wL})/(T_0 - T_S)$ dimensionless thermal efficiency based on the liquid temperature on the wall
$\Theta = (T_0 - T_{wa})/(T_0 - T_S)$ dimensionless thermal efficiency based on the gas temperature on the wall
ρ_0, ρ_S, ρ_L densities of the main flow, secondary flow, and liquid (kg/m^3)

Subscripts
0 parameter in the main flow
a air
ins insulation
L liquid
max maximal
min minimal
mx parameter in the mixture
S parameter in the secondary flow
w parameter under adiabatic-wall conditions

horizontal cylindrical channel, where the flow temperature was maintained constant, equal to ~150 °C. The existence of a limiting mass concentration, $(M_L)_{max} \approx 6\%$, was reported, above which the liquid content of the near-wall jet no longer affected the screen efficiency. In this case, the efficiency of the gas–liquid screen could be three times greater than that in the single-phase regime under identical dynamic and thermal conditions.

Experimental data on the efficiency of gas-droplet screens with moderate liquid concentrations (M_L = 5–10%) in a horizontal cylindrical channel were reported in [6]. In the same study, effects due to main-flow temperature and due to the structure of the thermal boundary layer were examined. Yet, for test channels arranged horizontally the question arises whether the liquid phase was distributed uniformly or not over the channel cross-section. In spite of the relatively high velocity of the gas flow ($U_0 \approx 30-50$ m/s), the influence of the gravity force on the cross-sectional distribution of large particles could be appreciable. The horizontal orientation of the channel could have a pronounced effect on the experimental data because it violated the symmetry conditions for the formation of the liquid film deposited onto the channel wall, which flowed down, under the action of the gravity force, from the upper into the bottom part of the channel.

In the present work, we experimentally examined the thermal efficiency of gas-droplet near-wall jets in a vertical cylindrical channel at relatively low concentrations of the liquid. The vertical orientation of the channel allowed us to avoid the asymmetric distribution of the liquid phase inside the channel.

2. Experimental setup and procedure

The experiments were performed on a setup whose schematic is shown in Fig. 1. The test section was a cylindrical channel of diameter D = 100 mm and length L = 1000 mm prepared from glass fiber plastic, a heat-insulating material. The thickness of the channel wall was h = 10 mm. The wall was additionally coated from

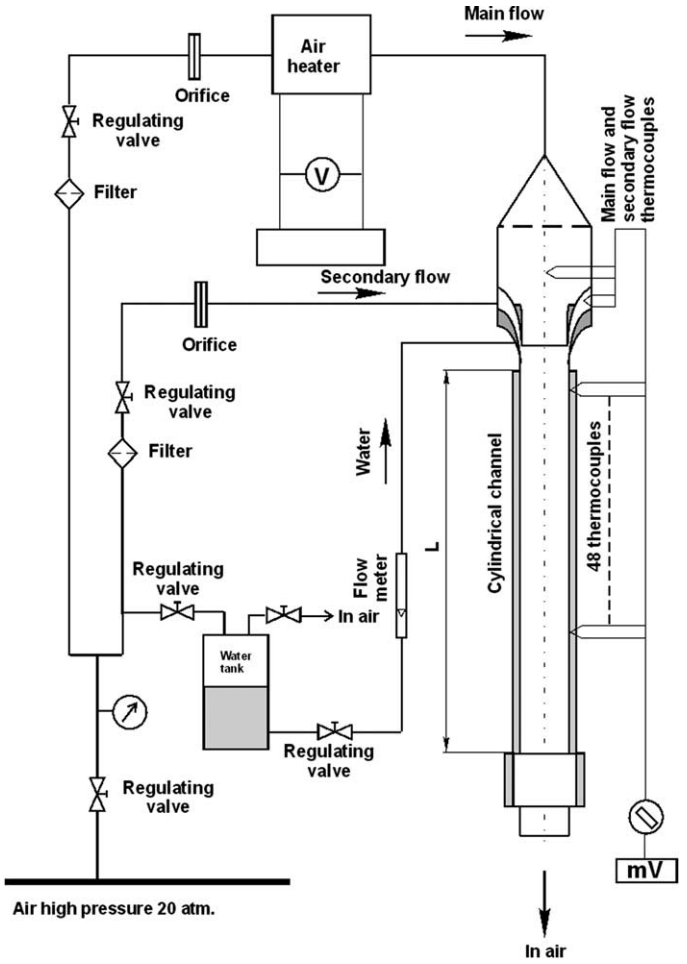

Fig. 1. Experimental setup.

outside with a foam–plastic layer of thickness $h_{ins} \approx 50$ mm to make the wall thermally insulated ($q_w = 0$). To measure the temperature of the insulated wall, the inside surface of the channel was provided with Chromel-Copel thermocouples installed over the entire length of the channel.

The co-axial stream formed in the mixing chamber (see Fig. 2) was supplied to the channel inlet. The stream

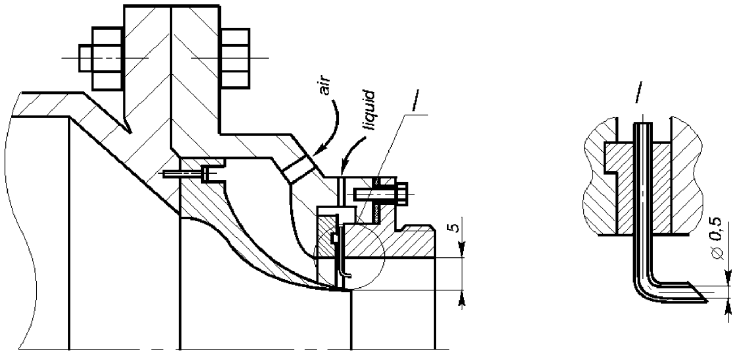

Fig. 2. Mixing chamber.

was made up by a single-phase central (main) flow injected through nozzle 1 (Fig. 2) and by a near-wall gas–liquid jet (secondary) flow. The main-flow temperature was a variable quantity. The secondary flow was supplied through an annular near-wall slot of height 5 mm, which was provided with 44 circularly positioned jet nozzles 2 (Fig. 2). These nozzles were used to atomize the liquid in the secondary flow. The estimated diameter of liquid droplets was ~200 μm; this diameter weakly varied both with the liquid-phase concentration and with the injection ratio. No large liquid drops were present in the flow.

The injection ratio, $m = \rho_S U_S/\rho_0 U_0$ was calculated from the mean rate of the coolant flow, which contained the gas–vapor phase and the liquid phase, where ρ_0 and U_0 are the density and velocity of the main flow, and $\rho_S U_S = (G_a + G_L)/A_S$, where A_S is the area of the annular slot, and G_a and G_L are the mass rates of the gas and liquid phase, respectively.

In the experiment, the variable quantities were the mass concentration of the liquid phase in the near-wall jet ($M_L = G_L/G_a = 0$, 0.016, 0.026, 0.05, and 0.1), the main-flow temperature ($T_0 = 20$–200 °C), and the injection ratio $m = 0.6$–1.8. Primary attention was paid to examining the deposition of liquid droplets onto the channel wall and the formation of the liquid film from the deposited droplets, which flowed down the channel wall in the co-current gas flow. The temperatures of the air and water supplied were roughly identical, equal to $T_S \approx 18$ °C. In the cases where the water and air temperatures slightly differed from each other, the coolant temperature was assumed to be equal to the mean temperature of the mixture; the latter temperature was found from the heat-balance relation as

$$T_S = \frac{G_a C_{p_a} T_a + G_L C_{p_L} T_L}{(G_a + G_L) C_{p_{mx}}} \quad (1)$$

Here G_a and G_L are the mass rates of the air and water flows in the near-wall jet, C_{p_a} and C_{p_L} are the specific heat capacities of the air and water prior to their jet mixing, and $C_{p_{mx}} = C_{p_a}(1 - M_L) + C_{p_L} M_L$ is the heat capacity of the air–water mixture in the jet flow.

To control the main-flow temperature, a 300-kW ohmic heater was used. The humidity in the main and secondary flows, measured phychrometrically at a temperature of 21 °C, was 3–4%.

In the majority of the experiments, the liquid phase was distilled water; for comparison purposes, several tests were performed with ethyl alcohol injected into the near-wall jet.

One of the main factors affecting the near-wall heat and mass transfer and the distribution of adiabatic-wall temperature is the diffusion- and migration-controlled deposition of liquid droplets from the turbulent near-wall jet flow, resulting in the formation of a liquid film on the channel wall. To examine the deposition pattern of the droplets, in the tests we measured the thickness of the deposited film and the mass rate of the film flow. This series of tests was performed under quasi-isothermal conditions. The experiments were carried out in another channel of identical diameter that consisted of individual pieces. Changing the total number of the pieces, we were able to very the total length of the channel. One of the pieces was provided with a capacitive probe flush-mounted with the wall.

This probe was used to measure the thickness of the liquid film formed by the droplets deposited onto the channel wall [7]. The main advantages of the capacitive method is the possibility of measuring the film thickness without introducing any disturbances into the flow pattern of the film flow, quasi-continuity of the measurements, and their high sensitivity and simple realization. The capacitive meter was designed according to the heterodyne scheme; it contained two high-frequency generators isolated in a special sensing device. To the drive circuit of the test oscillator, the co-axial capacitive probe was connected, installed in the measurement piece on the working surface of the channel. The diameter of the probe's outer electrode was 1.5 mm. The deposited liquid film acted upon the sensitive area of the probe, thus changing the frequency of the test oscillator. The output signal of the sensing device was the difference signal of the generators; that signal varied in proportion to the film thickness over the probe ($\Delta F(t) \equiv \delta$). The frequency versus time curve $\Delta F(t)$ could be converted into the thickness δ of the liquid film using the dependences $\delta = \Delta F(t)$ experimentally measured on a special device. The signal from the probe was fed into a capacity-frequency converter to be subsequently digitized and represented on the computer screen in graphical form as a test-generator frequency versus time curve. Thus, the present system allowed us to obtain the thickness of the liquid film as a function of time. Prior to performing the experiments, the probe was put to calibration tests in a special calibrating device on which known film thickness could be measured in the static regime. The system was tested in dynamic regimes by measuring downward film flows and comparing their characteristics with available theoretical dependences. The liquid-film thickness in the experiments ranged from 30 to 200 μm. The measurement error was not greater than 10%. The sampling length in the experiments was 2000 values sampled at a frequency of 500 Hz.

The mass rate of the liquid-film flow was measured by accumulating the liquid in a graduate through a 4-mm high annular slot.

The structure of the thermal mixing layer was studied by measuring the dry- and wet-bulb temperatures along the pipe radius. The dry-bulb temperature was measured by a thermocouple whose hot junction was shielded

from liquid droplets with a 3-mm diameter shield. The wet-bulb temperature was measured by a thermocouple with porous element. Prior to each temperature measurement at a certain point of the boundary layer, the bulb of the wet thermometer was sprayed with water from a dropper. Following this, the thermocouple indicated a temperature reduction during some time, and then a stationary temperature was reached. In the stationary regime, the temperature remained unchanged for a few seconds and then started rising sharply due to complete evaporation of liquid drops. The wet-bulb temperature was assumed to be equal to the sensor temperature in the stationary regime.

From measured temperature profiles, distributions of relative humidity and mass concentration of water vapor were calculated. The humidity was calculated by the well-known procedure described in [8,9].

The profiles were measured in three cross-sections of the channel, 40, 240, and 440 mm from the inlet to the test section; these values corresponded to the values of the dimensionless parameter x/S equal to 8, 48, and 88.

3. Preliminary experiments

First of all, preliminary tests were performed on the experimental setup to determine the main characteristics of its test section. In those tests, profiles of time-average flow velocity and temperature, and also the turbulence number, were measured in the inlet cross-section of the working channel and in several cross-section of the channel at various distances from the inlet.

The profiles of time-average flow velocity profiles along the radius of the central nozzle are shown in Fig. 3(a). The measurements were performed at a distance of 0.5 mm from the nozzle at mass-average flow velocities U_0 of 10.2, 22.5, and 30.3 m/s. It is seen from the figure that the profiles are almost coincident, and in the central part of the flow there is a potential flow core with an almost uniform velocity distribution. The thickness of the boundary layer at the exit plane of the nozzle is not greater than 4.5 mm.

The turbulence-number distributions are shown in Fig. 3(b). In the main-flow core, the turbulence number is about 1%, whereas in the boundary layer the turbulence number runs into 10–13%. The data show that the core flow is a low-turbulence one.

The radial distribution of the main-flow temperature in the channel at the nozzle exit plane was also uniform within 2.5% (in the temperature range 30 to 200 °C). The thickness of the boundary layer was roughly equal to the thickness of the dynamic layer.

The flow velocity profiles were measured at three cross-sections, $x = 0.5$, 45, and 243 mm from the nozzle exit plane. The mean velocity was $U_0 \cong 27$ m/s, and the Reynolds number was $Re = 1.56 \cdot 10^6$.

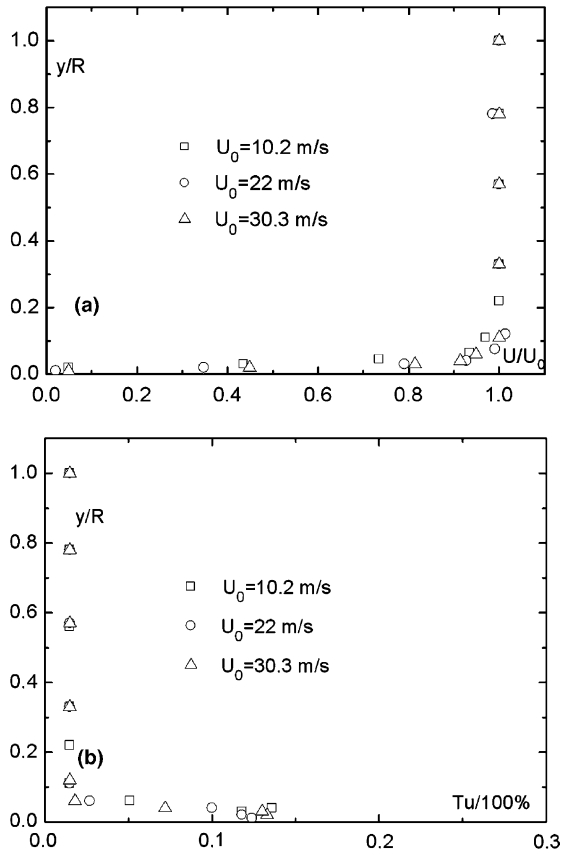

Fig. 3. Profiles of time-average flow velocity (a) and turbulence number (b) in the outlet plane of the central nozzle.

The profile of time-average flow velocity over the length of the cylindrical channel is shown in Fig. 4(a). The injection of the near-wall jet into the boundary layer gives rise to some deformation of the velocity profile. At a distance of 0.5 mm from the injection place, a distinct boundary between the main flow and the near-wall flow is observed. This boundary rapidly smears in the downstream direction, and at a distance of 243 mm from the injection place the velocity profile becomes turbulent and completely filled.

The distribution of the turbulence number along the channel diameter and the variation of the turbulence of the mixing flows along the channel length are shown in Fig. 4(b). It is seen from the figure that the effect of the separating boundary rapidly vanishes in the downstream direction, and the flow becomes uniform. The maximum measured turbulence number is 12%.

The time required for the equilibrium thermal regime to be established in the experimental setup was determined by multiple measurements of the adiabatic-wall temperature, performed over a long time interval, with the rates and temperatures of the main and secondary

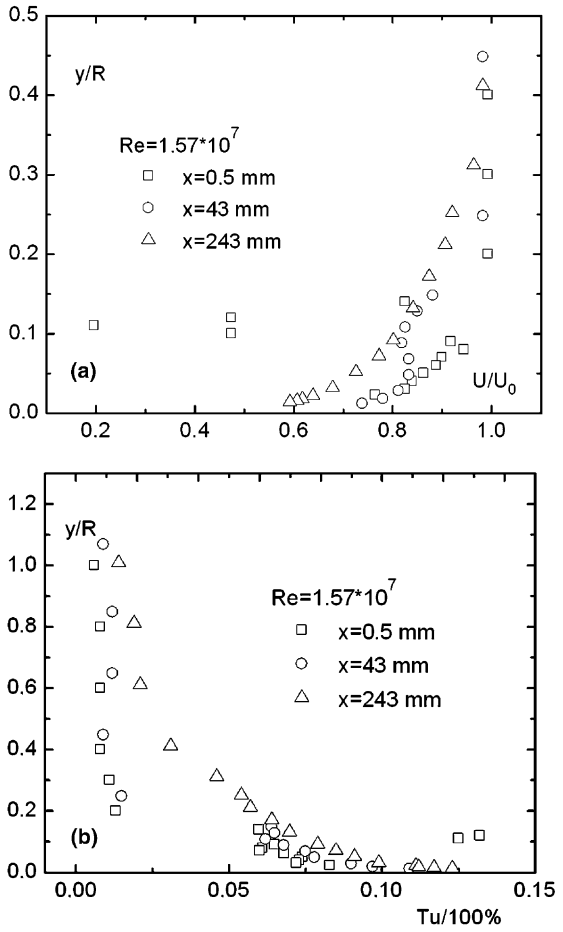

Fig. 4. Variation of flow velocity (a) and turbulence number (b) profiles over the length of the test section, $m = 1$.

airflows kept unchanged. The indications of the thermocouples were registered each hour. The time interval required for the thermal equilibrium to be attained was found to be not shorter than an hour. In the established regime, the results admitted generalization in the universal coordinates (see Fig. 5) by the well-known Kutateladze–Leont'ev equation for near-wall single-phase screens [10]:

$$\Theta = \left[1 + 0.25 Re_S^{-0,25} \frac{x}{mS}\right]^{-0.8}, \tag{2}$$

where

$$\Theta = \frac{T_0 - T_w}{T_0 - T_S} \tag{3}$$

is the thermal efficiency of the gas screen, T_0 is the main-flow temperature, T_w is the adiabatic-wall temperature, and T_S is the coolant temperature. In formula (2), Re_S is the Reynolds number based on the slot height and U_S is the gas velocity at the slot exit plane.

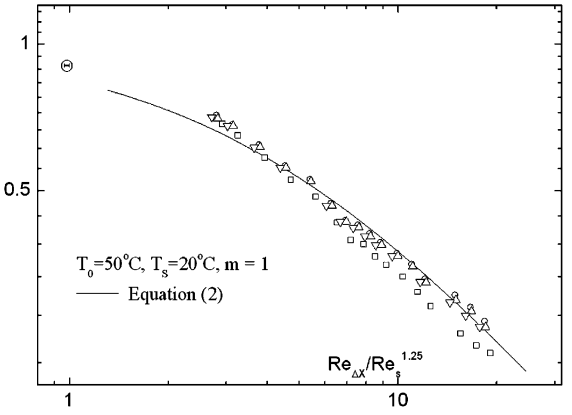

Fig. 5. Comparison of experimentally measured thermal efficiencies with the Kutateladze–Leont'ev curve.

Thus, in the single-phase regime, a good agreement with classical dependence (2) on the thermal efficiency of screens was obtained, indicative of the absence of any methodical error in the devised experimental setup.

4. Experimental data on the deposition of the liquid

A main specific feature of near-wall gas-droplet jets is deposition of liquid droplets on the adiabatic channel surface. In view of this, at the first stage of the experimental study we examined the regularities of the deposition process, the thickness and regime of the film flow, and also the effect of the co-current flow on the characteristics of the liquid-film flow. The tests were conducted in nearly adiabatic regime ($T_S \approx T_0$); the results gained in this series of tests were described in [11].

Variation of the flow rate $\Gamma = G_L/\rho_L \cdot \pi D$ due to the liquid droplets deposited onto the wall over the length of the channel at various concentrations of the liquid phase and various velocities of the co-current flow is shown in Fig. 6. The experimental data here are given in the form of the Γ/Γ_S ratio presenting the fraction of the deposited liquid in the total specific mass of the liquid phase supplied in the atomized form through the annular slot at the entrance to the channel.

For co-current two-phase jets (Fig. 6(a)), the rate of droplet deposition attains its highest at the lowest concentration of the liquid ($M_L = 0.016$ and 0.026), and almost all droplets undergo deposition onto the channel wall over rather short a length ($x/S = 60$–100). With increasing concentration of the liquid phase in the near-wall jet ($M_L = 0.05$–0.1), the rate of droplet deposition decreases, and only 40–50% of the initial liquid content of the injected jet flow gets deposited onto the wall by the time the flow reaches the channel exit.

As the velocity of the co-current main flow increases (Figs. 6(b) and (c)), the film flow becomes unstable. The

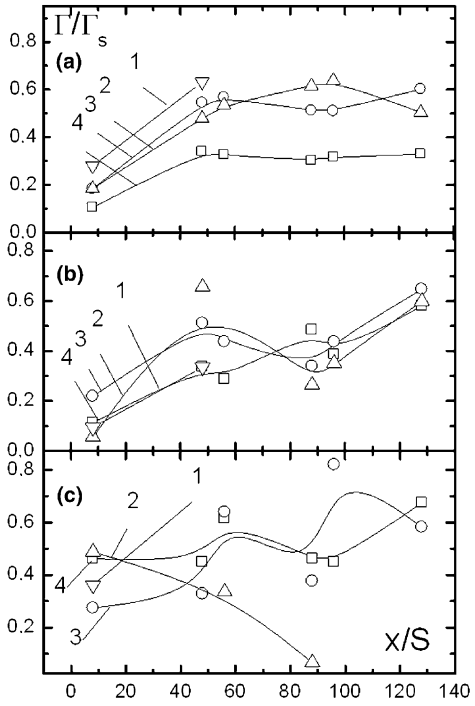

Fig. 6. Relative flow rate for the film deposited on the channel wall. Injection ratio: (a) $m = 1.8$, (b) 1.0 and (c) 0.6. $T_0 \approx T_S \approx 20$ °C. 1—$M_L = 0.016$; 2—0.026; 3—0.05 and 4—0.1.

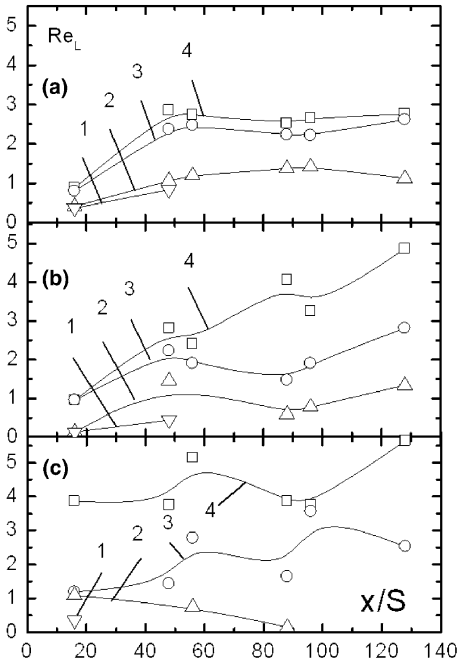

Fig. 7. Variation of the Reynolds number of the liquid film deposited from the near-wall gas-droplet jet. Designations are the same as in Fig. 6.

decay of the Γ/Γ_S ratio along the channel length is indicative of partial stalling of the liquid film, followed by its re-attachment to the wall. Visual observations over the flow at these regimes provide further evidence for this. In the cases of stalled film flows, rivulet regimes were observed.

Fig. 7 demonstrates the behavior of the film Reynolds number $Re_L = \Gamma/\nu_L$ under the adopted experimental conditions. It was found that maximum Reynolds numbers $Re_L < 5$; for gravity film flows, such Reynolds numbers correspond to the no-wave flow regime. Yet, the flow here is a wavy one due to the action of the co-current flow and due to possible disturbances introduced into the film flow by the collisions of liquid droplets with the film surface. Indicative of this are instantaneous measured values of the thickness of the film flow shown in Fig. 8. It follows from the figure that even with no external flow (Fig. 8(a)) the film surface is wavy, the amplitude and velocity of the waves increasing with increasing velocity of the co-current flow (Fig. 8(b)–(d)). According to Phillips [12], who examined the wave formation processes on deep water, the high-frequency part of the spectrum has the form $\Phi(t) = C_1 g^2 F^{-5}$, where C_1 is some empirical constant, g is the free-fall acceleration, and F is the frequency. Fig. 8(g) and (h) show that the dependence $\Phi \sim F^{-5}$ in the high-frequency portion of the spectrum is also exhibited by the wave formation processes in thin films formed from gas-droplet flows; this observation is indicative of nonlinear nature of the wave process under study.

5. Thermal efficiency of gas-droplet screens

Variation of adiabatic-wall temperature over the channel length for fixed inlet liquid-phase concentration $M_L = 0.016$ at the injection ratio $m = 0.6$ is shown in Fig. 9. In this series of experiments, the variable parameter was the main-flow temperature, $T_0 = 30$–200 °C. Note specific features of the data in Fig. 9. In the initial cross-sections of the channel the wall temperature decreases due to the intense evaporation processes due to which the liquid deposited onto the channel surface acquires the adiabatic-evaporation temperature [13]. Then, the wall temperature starts increasing, and its distribution becomes unstable owing to the stalling of the film flow from the wall. The effects are manifested most brightly at high main-flow temperatures ($T_0 > 100$ °C); the experimental points here lie close together, showing that the effect due to flow heating on the thermal efficiency of the screen in this range of temperatures is weak.

The experimental data of Fig. 9, presenting the thermal efficiency (3) as a function of the universal parameter

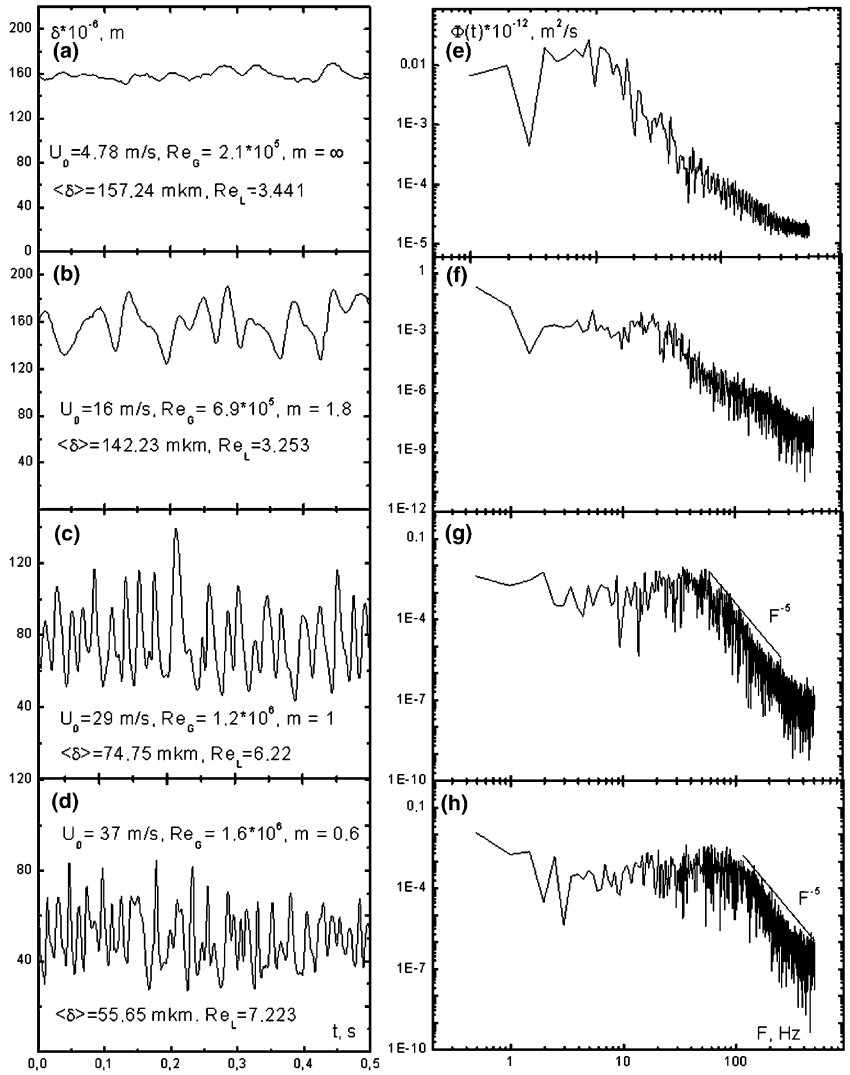

Fig. 8. Instantaneous thickness of the deposited liquid film ((a)–(d)) and the corresponding frequency spectra ((e)–(h)) at the distance $L = 644$ mm flow the injection place. Mass concentration of the liquid in the near-wall jet, $M_L = 0.1$.

in the form (2) widely used in the theory of single-phase gas screens, are shown in Fig. 10. The experimental points are seen to exhibit a scatter that depends on the air temperature in the main flow. The highest efficiency here is achieved at low temperatures of the main flow. The wall cooling effect, i.e., the temperature reduction due to the evaporation of the liquid phase on the wall, results in that the quantity $\Theta > 1$ is observed almost throughout the entire length of the channel, and only at relatively high temperatures the experimental data gradually approach the single-phase regime. In the latter case, it is the evaporation processes in the flow core that starts playing a decisive role. The thermal efficiency in the two-phase regime can be more than five times greater than that in the single-phase regime.

The liquid films formed on the channel wall evaporates into the boundary-layer flow and, under the conditions of no heat exchange with the wall, the wall temperature can be expected to acquire the adiabatic-evaporation temperature. Using the data of Fig. 9, one can estimate the maximum experimental and predicted efficiencies of the thermal screen in the two-phase regime:

$$\Theta_{\max} = \frac{T_0 - (T_w)_{\min}}{T_0 - T_S}, \tag{4}$$

where the temperature $(T_w)_{\min}$ is the adiabatic-evaporation temperature T_0^* at the temperature of the main flow and zero humidity (solid curve in Fig. 11) or the equilibrium temperature T_S^* of the vapor–gas-droplet mixture

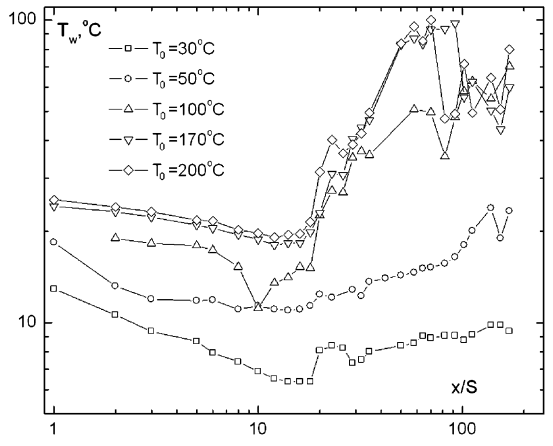

Fig. 9. Distribution of adiabatic-wall temperature over the length of the cylindrical channel. $M_L = 0.1$; $m = 0.6$.

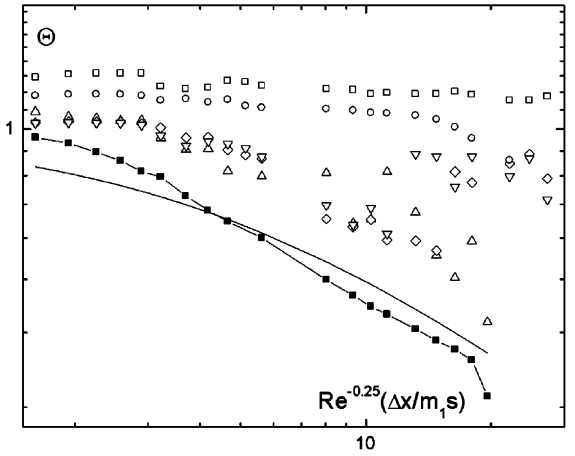

Fig. 10. Representation of the experimental data on the thermal efficiency of two-phase screens in the generalized coordinates, $m = 0.6$; $M_L = 0.016$. Curve—formula (2), full symbols—single-phase regime. Other symbols are the same as in Fig. 9.

at the slot exit plane (dashed curve in Fig. 11). The experimental data of Fig. 11 fall in the region between these calculation data. The latter shows that, actually, the deposited liquid film evaporates into the mixing layer of the main flow and the secondary flow injected through the peripheral slot.

6. Comparison of experimental data with numerical results

The experimental data were compared with modeling results obtained by the model described in [14] and in the first part of the present article (see [15]).

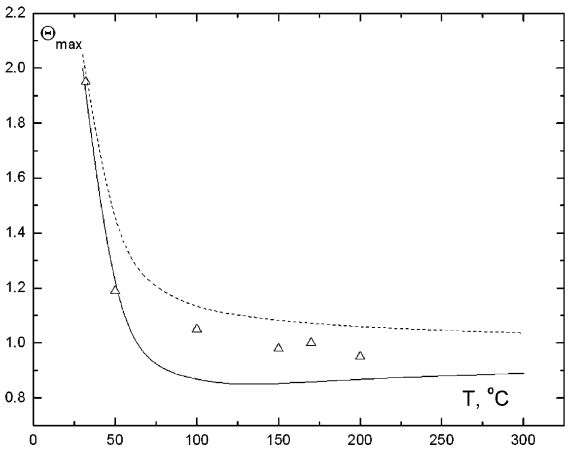

Fig. 11. Maximum value of the efficiency parameter for the two-phase jet, $m = 0.6$; $M_L = 0.016$. Points—experiment; curves—thermal efficiency Θ_{max} calculated from the temperatures T_0^* and T_S^* (solid and dashed curve, respectively).

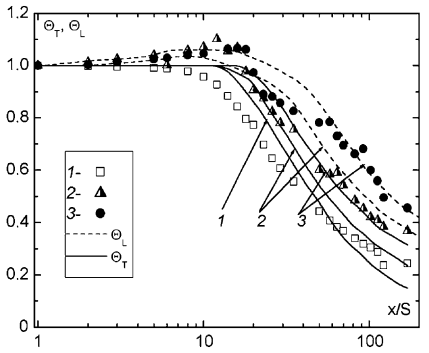

Fig. 12. Comparison of the experimental data on the thermal efficiency of the gas-droplet screen with the numerical results obtained by the model of [14]. $T_0 = 100$ °C. 1—single-phase regime; 2—$M_L = 0.016$; 3—$M_L = 0.026$; dashed curve—the temperature T_w in formula (2) is taken equal to the liquid-phase temperature on the wall; solid curve—the temperature T_w is taken equal to the gas-phase temperature.

The measured and predicted thermal efficiencies Θ for various inlet liquid-phase concentrations are compared with each other in Fig. 12. As the determining temperature in this and subsequent graphs, the wall temperature at the slot position is taken. In this way, we were able to exclude from the consideration the complex thermogasdynamic processes that proceeded inside the slot channel. The numerical data were obtained for two cases: in the first case the wall was assumed dry, and in the second case the wall assumed to be covered by the liquid film whose temperature was equal to the liquid-phase temperature. As it is seen, the data obtained

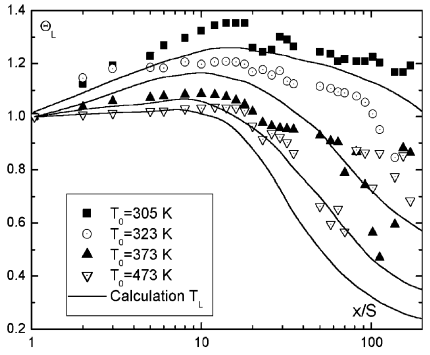

Fig. 13. Effect of main-flow temperature on the thermal efficiency of the gas-droplet screen. $M_L = 0.016$; $m = 0.6$.

in the second case provide a better agreement with the experimental data.

Over the initial length of the channel ($x/S < 40$), we have $\Theta > 1$; this result lends support to the previously noted cooling effect, which was found to be more pronounced in regimes with higher concentrations of the droplet phase.

All subsequent calculations of thermal efficiency were performed based on the liquid-phase temperature on the wall. The effect of main-flow temperature on the value of Θ_L is analyzed in Fig. 13. Despite the considerable scatter of experimental points, the numerical analysis generally well reflects the experiment. As it is seen in Fig. 10, an increase in the main-flow temperature results in worsened protective properties of near-wall gas-droplet screens. The latter regularity can be explained by the fact that the growth of temperature intensifies the evaporation processes far from the wall, thus decreasing the droplet content in the near-wall zone.

An important parameter in organizing thermal protection of surfaces by near-wall jets is the ratio of mass velocities of the near-wall jet and the main flow. Fig. 14 illustrates the effect of this parameter on the thermal efficiency of near-wall gas-droplet screens.

Note the following general tendency in variation of Θ_L with the parameter m. Both the experimental and predicted dependencies are indicative of rather weak influence of the injection ratio on the thermal efficiency Θ_L. The experimental data show that, for all investigated values of m, $\Theta_L > 1$ almost over the whole surface of the channel. The exception is regimes with $m < 1$; in this case, the thermal efficiency at the outlet of the channel starts decreasing. It should be stressed that the numerical calculations yield a more intense decrease of Θ_L in outlet cross-sections; this result calls for further analysis.

Thermophysical properties of the liquid phase may have an appreciable effect on heat and mass transfer in near-wall jets and on their thermal efficiency. In all previous experiments, the working liquid was water. For comparison, a series of tests was performed in which ethanol was used as the working liquid. The experimental and numerical results on the variation of adiabatic-wall temperature with water or ethanol injected in the main flow are shown in Fig. 15. Here, all the thermogasdynamic conditions at the inlet to the channel were identical.

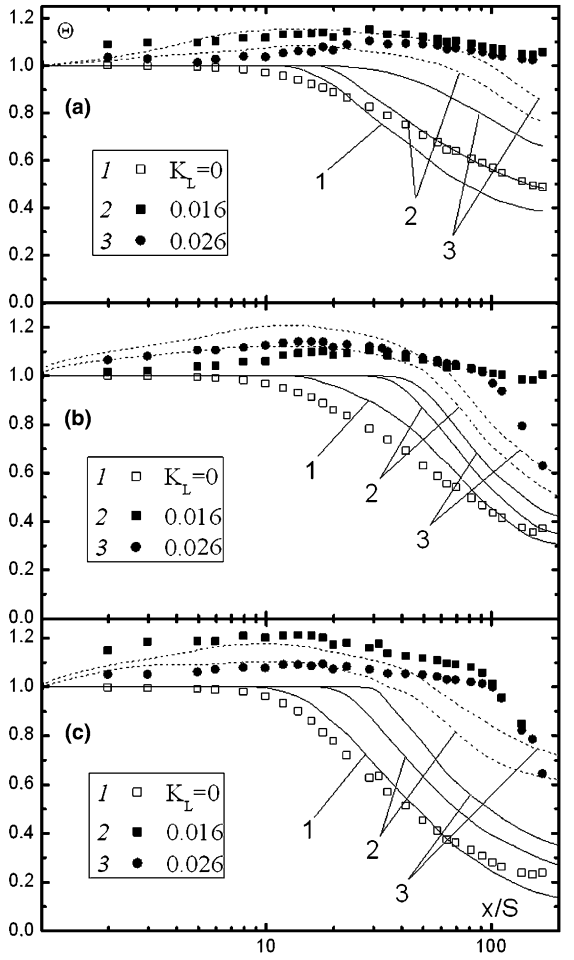

Fig. 14. Effect of injection ratio on the thermal efficiency of the gas-droplet screen. $T_0 = 50$ °C, (a) $m = 0.6$; (b) $m = 0.8$; (c) $m = 1.6$.

As it is seen from Fig. 15, in the case of ethanol, whose boiling point is much lower than that of water, the wall temperature first is much lower than in the case of water. Yet, farther downstream, at $x/S > 10$, the droplets undergo rapid evaporation due to lower heat of vaporization, and the data for the two-phase jet with ethanol droplets approach the single-phase regime.

All the above-mentioned specific features in the behavior of near-wall jets with different heat carriers affect the magnitude of the thermal-efficiency parameter. This conclusion can be drawn from Fig. 16, where relevant data are shown. As it follows from Figs. 15 and 16,

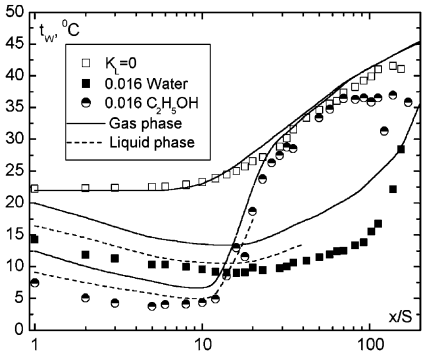

Fig. 15. Effect of physical properties of the vapor–liquid component on the distribution of adiabatic-wall temperature, T_0 = 50 °C.

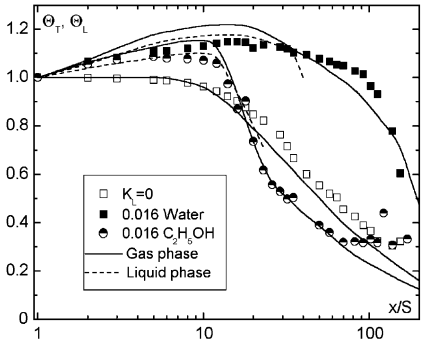

Fig. 16. Effect of thermophysical properties of the vapor–liquid component on the thermal efficiency of the gas-droplet screens, T_0 = 50 °C.

the predicted values well correlate with the experimental ones.

7. Conclusions

In the present study, an experimental dataset concerning the thermal efficiency of near-wall gas-droplet jets was obtained. In the experiments, the variable quantities were the liquid-phase concentration, the flow-core temperature, the injection ratio, and the thermophysical properties of the liquid. A low additive of the liquid phase (not more than 1.6%) is shown to result in an appreciable (by 3–5 times) improvement of the protective properties of two-phase screens. An increase in the main-flow temperature worsens the screen efficiency parameter. A characteristic feature of two-phase jets is regimes with $\Theta > 1$; such regimes are possible due to the evaporation processes that proceed directly on the channel surface. The use of a low-boiling heat carrier (ethanol) first results in an increase of the thermal efficiency and, then, in an abrupt fall of this quantity due to intensification of evaporation processes.

Acknowledgments

This work was supported by the Program of the President of the Russian Federation for Supporting Leading Scientific Schools (Grant No. 1308.2003.8) and Russian Academy Program (project 3.5.2.). M.A. Pakhomov also thanks the Russian Foundation for Supporting National Science for the grant for Young PhD Scientists-2004. K.A. Sharov expresses his gratitude to the Russian Foundation for Basic Research for Grant No. 01-02-16994MAC for Young Scientists-2004.

References

[1] E. Talmor, N. Weber, Foreign-gas film cooling along non-converging and converging walls at various free-stream turbulence levels, Proc. IV Int. Heat Transfer Conf., Paris, France FC-8.7 (1970) 1–11.
[2] V.M. Repukhov, A.I. Neduzhko, Effect of non-equilibrium heat and mass transfer on the thermal efficiency of gas–vapor–liquid screens, Proc. Acad. Sci. Ukrainian SSR 2 (Ser. A) (1991) 63–66 (in Russian).
[3] V.M. Repukhov, A.I. Neduzhko, Thermal efficiency of gas–vapor–liquid screens behind tangential and inclined slots, Promyshlennaya Teplotekhnika 4 (1989) 31–37 (in Russian).
[4] V.M. Repukhov, Thermal efficiency of non-equilibrium gas–vapor–liquid screens, Promyshlennaya Teplotekhnika 6 (1986) 11–19 (in Russian).
[5] E.P. Volchcov, V.P. Lebedev, V.I. Terekhov, N.E. Shishkin, Experimental study of the effect of concentration of dispersed liquid droplets on the thermal efficiency of gas screens, Siberian Phys.-Techn. J. 1 (1992) 28–32 (in Russian).
[6] V.I. Terekhov, K.A. Sharov, N.E. Shishkin, An experimental study of gas–stream mixing with a near-wall gas-drop jet, Thermophys. Aeromech. 6 (1999) 331–339.
[7] S.V. Krotov, A.D. Nazarov, A.N. Pavlenko, A.F. Serov, A capacitive probe for measuring local film thickness, Pribory Tekhnika Eksperimenta 1 (1997) 149 (in Russian).
[8] M.A. Berliner, Measurements of Humidity, Moscow, Energy, 1973 (in Russian).
[9] D.P. Bespalov, V.N. Kozlov, L.T. Matveev, Humidity Table, Leningrad, Gidrometeoizdat, 1972 (in Russian).
[10] S.S. Kutateladze, A.I. Leont'ev, Heat and Mass Transfer in Boundary Layer, Hemisphere, New York, 1989.
[11] V.I. Terekhov, A.F. Serov, K.A. Sharov, A.D. Nazarov, Experimental investigation of the deposition of liquid droplets on the wall of a vertical cylindrical channel from wall gas-droplet jets, High Temp. 41 (5) (2003) 639–645.
[12] O.M. Phillips, On some properties of the spectrum of wind-generated ocean waves, J. Marine Res. 16 (1958) 231–245.

[13] B.F. Boyarshinov, E.P. Volchkov, V.I. Terekhov, Heat and mass transfer with liquid evaporation into gas flow, Russ. J. Eng. Thermophys. 1 (1) (1991) 93–112.

[14] V.I. Terekhov, M.A. Pakhomov, Numerical investigation of the thermal efficiency of a two-phase gas-droplet wall screen in a cylindrical channel, High Temp. 40 (4) (2002) 586–593.

[15] V.I. Terekhov, M.A. Pakhomov, Thermal efficiency of near-wall gas-droplets screens. I. Numerical modeling, Int. J. Heat Mass Transfer, in press, doi:10.1016/j.ijheatmass-transfer.2004.11.010.